2004

Latent-image formation in tabular AgBr grains: simulation studies

Richard Hailstone

Rene DeKeyzer

Recommended Citation
Imaging Science Journal 52N3 (2004) 164-175

Latent-image formation in tabular AgBr grains: simulation studies

R K Hailstone[a]* and **R De Keyzer**[b]
[a]Chester F. Carlson Center for Imaging Science, Rochester Institute of Technology, 54 Lomb Memorial Drive, Rochester, NY 14623, USA
[b]R&D Materials Research, Agfa-Gevaert Group, Septestraat 27, B2640 Mortsel, Belgium

Abstract: A simulation programme based on the nucleation-and-growth model of latent-image formation was used to study how trap depth and trap density at various tabular grain thicknesses affected quantum sensitivity and reciprocity failure. Using a 1.2×0.2 μm model 'grain', the unsensitized case was simulated with 0.05 eV traps located on both the face and the core of the grain, the latter to simulate the effect of twin planes on latent-image location. The trap densities were adjusted to achieve a higher internal speed than surface speed, as seen experimentally with the emulsion used to validate the simulation. To simulate the effects of chemical sensitization, these parameters were held fixed while edge traps of depths 0.2–0.6 eV were added at various trap densities for grain thicknesses of 50, 100 and 200 nm. All but the lowest trap densities at 0.2 eV changed the situation to complete or almost complete edge domination for latent-image location. Maximum efficiencies for latent-image formation were six to eight absorbed photons/grain for a 0.01 s exposure, although the trap density had to be decreased as the trap depth increased to achieve these maximum values. A decrease in efficiency with decreasing thickness as well as with decreasing diameter was seen for the lower trap depth values. These grain diameter and thickness effects disappeared for simulations using a 10^{-6} s exposure, indicating that the decreasing efficiency at 0.01 s was due to differences in the onset of low-irradiance reciprocity failure. Reciprocity failure was simulated for chosen trap depth/density combinations. These data were compared with experimental reciprocity failure data to help validate the model. Reasonable agreement was obtained for trap depths in the range of those deduced from the experimental phase of the project. However, uncertainties regarding other parameters that affect the position of the reciprocity failure curve with respect to exposure time must be reduced before this agreement can be considered a validation of the model.

Keywords: AgBr, tabular grain, computer simulation

1 INTRODUCTION

The use of tabular grains has become pervasive in silver halide image capture systems.[1] Recent work has suggested significant imaging advantages from reduced grain thickness, leading to ultrathin grains with thicknesses appreciably <100 nm.[2] The implications for the efficiency of latent-image formation in such thin grains have yet to be addressed systematically. This paper, along with a companion paper giving experimental results for tabular grains with different thicknesses,[3] is an attempt to address this issue.

Previous simulation studies of the efficiency of latent-image formation in tabular grains have not considered size effects. Rather, they have concentrated on the trap density and depth required to image efficiently. In a study of a 1.0×0.2 μm AgBr tabular 'grain', it was found that traps located at the corners of the grain and varying in depth between 0.2 and 0.6 eV

The MS was accepted for publication on 12 January 2004.
* *Corresponding author: Chester F. Carlson Center for Imaging Science, Rochester Institute of Technology, 54 Lomb Memorial Drive, Rochester, NY 14623, USA; e-mail: hailstone@cis.rit.edu*

 IMAG 1303 © RPS 2004 DOI: 10.1179/136821904225011645

provided no clear advantage over 0.2 eV traps uniformly distributed over the grain surface, as long as the minimum developable size was three atoms.[4] This result was despite the corner traps' having a trapping radius twice that of the uniformly distributed traps. The assumption of a minimum size of three atoms is reasonable for emulsions sensitized with sulphur and gold, and optimally developed. However, if the minimum developable size is four atoms, as might be the case for less than optimal development, there is some efficiency advantage to limiting the traps to corner locations, particularly at high irradiance.

Another simulation study focused on the effect of a 10% iodide core in the same size AgBr grain as above.[5] The internal iodide centres are energetically disposed to trap holes.[6] However, their ability to decrease recombination depends upon the time scale of the formation of an interstitial silver ion from a lattice silver ion adjacent to the iodide-trapped hole, which reduces the recombination radius. The time scale for this process is uncertain. This was simulated considering a range of recombination radii for the iodide-trapped hole. Both uniform and non-uniform placement of surface traps intended to mimic chemical sensitization centres were studied. The iodide core with small recombination radii for the iodide-trapped holes led to an efficiency advantage when uniformly distributed 0.2 eV traps were at the surface. However, a bimodal distribution of traps in which the minority population had a 0.4 eV trap depth and located at the grain corners/edges gave high efficiency with or without the iodide core, provided such traps had a trapping radius twice that of the 0.2 eV traps forming the majority population.

In these previous simulation studies, only general considerations were given to the body of experimental data on tabular-grain emulsions. One reason for this casual approach is that the available experimental data are quite meagre.[7,8] What is needed for gauging the meaningfulness of the simulation results is sensitometric data, such as reciprocity failure and quantum sensitivity (QS), on well-defined emulsions. Unfortunately, such data are not generally available in the published literature. The present study has attempted to remedy this situation by collecting and publishing such data in a companion paper.[3] These data have been used both to establish some parameters in the model and to provide data with which to validate the model.

The next section describes the methodology employed in the simulations. Then data which map QS space as a function of grain diameter and thickness for a wide variety of trap depths and densities are presented. These data are then used in the validation stage, in which a given set of experimental data is fitted with chosen simulation parameters. The significance of the experimental fitting in light of remaining uncertainties about simulation parameters is then discussed. Finally, the conclusions of the present work are stated.

2 METHODOLOGY

2.1 General simulation description

Details concerning the simulation programme can be found elsewhere.[9,10] Here, a brief review is given. The simulation uses a Monte Carlo approach to follow the absorption of photons, movement of charge carriers, trapping and detrapping of electrons and holes, formation and decay of silver atoms, nucleation and growth of latent sub-image and latent image, and recombination between electrons and holes. These processes are all carried out within a model space meant to simulate the size and shape of the emulsion grains being studied.

The simulation is initiated by defining the length, width and height of the model space. The model space for the current project is shown in Fig. 1. Also, the parameters defining any interior boundaries, such as twin planes or high-iodide regions, can be specified. Then, the trap locations must be specified, as well as their depth and trapping cross-section. The present case, where tabular grains are of interest, differentiates between traps located on the large faces, on the edge and in the interior of the grain at the twin planes.

Photon absorption can be either a volume or a surface process, depending on the problem under study. In either case, the location of the photon absorption is randomly chosen, and it is at this point that the random walk of the electron and hole begin. Input parameters specify the mean distance per jump of the carriers, and this is usually adjusted to be about 20% of the smallest grain dimension for the electron.[10] Because of its lower mobility, due to more and deeper trapping,[10] the hole has a mean jump distance 1/100 that of the electron. The distribution of actual jump distances follows that of a Gaussian probability distribution.

In principle, after each carrier jump, the possibility of trapping or recombination should be checked. But partitioning of the grain into regions allows for more

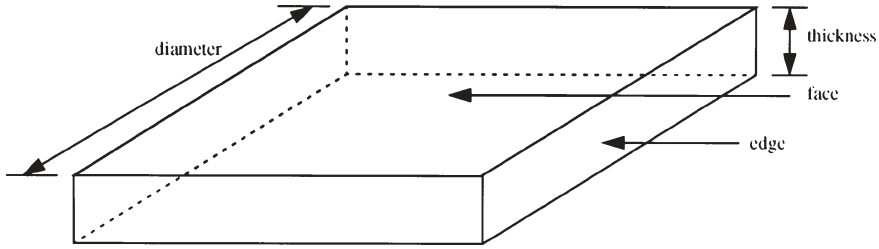

1 Model space for simulations, showing 'square' tabular grain

efficient simulations because checks for trapping or recombination only need be done in those regions where there is a finite probability of the event occurring.[5] Trapping or recombination occurs when the trajectory of the free carrier passes through a sphere whose diameter is determined by the trapping or recombination radius. Upon trapping, the lifetime of the carrier in the trap is determined by the trap depth and attempt-to-escape frequency.

Trap location can be either explicit or implicit for electron traps. In the present study, both modes are used, for reasons to be described in the next section. In the explicit mode, the trap coordinates are specified, and trapping occurs as described above. In the implicit mode, a trapping probability is calculated based on the density of traps and their cross-sections. When the electron jump is such that it is within a trap radius of such traps, or its jump has caused it to pass through such a region, it is trapped based on this probability and a selected random number. In the case of hole trapping, this only occurs at the surface in the present study, and the density of hole traps (negative kink or kink-like sites) is assumed to be high enough for there to be a unit probability of trapping whenever the hole is within a trap radius of the surface.

Also, upon electron trapping, an atom formation time is determined. This value is directly correlated with the ionic conductivity of the grain.[9] If the atom formation time is shorter than the trap escape time, atom formation will be favoured. Otherwise, escape to the conduction band will dominate. The time for both events is determined by an exponential probability distribution.[10] Upon atom formation, an atom lifetime must be calculated. Decay of the silver atom competes with electron trapping to form a two-atom centre, the nucleation event. For formation of two-atom and larger centres, the capture of the interstitial silver ion is assumed to be fast and is not explicitly followed. Some of these concepts are illustrated schematically in Fig. 2.

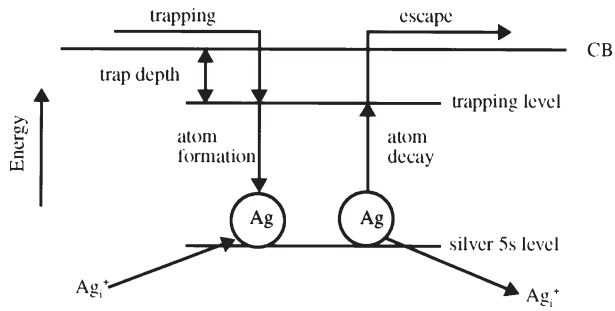

2 Schematic illustrating reversible processes followed in simulation

There are two pathways for recombination: between free electrons and trapped holes and between free holes and trapped electrons. Usually, the former pathway dominates because of the low mobility of the hole. However, upon chemical sensitization, deeper and more numerous electron traps are formed. At some trap depth/density combination, latent-image formation efficiency decreases because free-hole/trapped-electron recombination begins to increase. This situation is called *oversensitization*.[11,12] This alternative pathway does not include recombination between a free hole and an electron trapped at a silver ion (a silver atom), because it is assumed that a silver atom is located at a positively charged site and would therefore repel holes.

When all the electrons are consumed by the irreversible processes of nucleation, growth or recombination, the simulation of one grain is completed. But, because all the processes are random, the final state of that grain may or may not be that of the mean response of the grains in an emulsion. So, the entire simulation process must be repeated many times, each with a different seed for the random number generator, to achieve a mean response which can be compared with experimental data. For this reason, simulation on a parallel processor is highly advantageous.[10] Following the simulation over the specified number of 'grains',

the fraction of grains developable F is determined. Then, the photon level is incremented and the entire process repeated to achieve an F–log P curve, where P is the mean number of absorbed photons/grain.

2.2 Specifics for current simulation study

Simulations based on the above procedure lead to reciprocity failure curves which have slopes at the low-irradiance end that are steeper than one sometimes finds experimentally. This was particularly true for the tabular grains of this study. The lower experimental slopes are often attributed to some unspecified inherent hole removal process which reduces recombination,[13] favouring more efficient nucleation and less low-irradiance reciprocity failure (LIRF). A hole removal process can be incorporated into the simulations to achieve a better fit with the experimental data, but this often leads to a plateau in the LIRF region that is not seen experimentally.[13]

There are, in fact, several possible mechanisms of hole removal which could affect the LIRF slope. There may be temporary hole traps in the grain which do not act as recombination centres. In addition, hole-removing silver clusters might unintentionally form during emulsion precipitation. Also, the gelatin itself has the ability to react with photogenerated halogen.[14] Counteracting these various processes which reduce recombination is the possibility of intergrain rehalogenation which would increase recombination and also the LIRF slope.[15]

Considering all these processes, it is not surprising that a simple hole removal event does not adequately lead to accurate simulations. The present study has included two additional parameters which will allow an empirical adjustment of the LIRF slope to match that seen experimentally. Normally, the time scale on which the hole removal process occurs is given by the mean hole removal time. In the new scheme, this mean time is increased when a certain exposure time is reached, and the factor by which it is increased is also a parameter. When the exposure time is increased in a reciprocity study, usually by a factor of 10, this factor is again applied to increase the hole removal time further, and so on for each additional increment in the exposure time. This procedure minimizes the onset of the LIRF plateau described above. Although simply an empirical fitting approach, this procedure is meant to capture all the complexity of the various processes affecting the LIRF slope.

Another modification needed in the current project was related to the explicit versus implicit trap checking described above. Normally, implicit checking is used because this leads to faster simulations. But, in tabular grain simulations, preliminary work suggested that trap densities at the grain edge might need to be very low to achieve a correct simulation. Further work showed that, although the implicit method at low trap densities gives the same QS at high irradiance as the explicit method, the implicit method gives LIRF onsets at longer times than the explicit method did, so an algorithm had to be developed for explicit trap checking in the case of those traps located on the edge of the grain.

A further aspect, just alluded to, is the assumption that the important traps in the case of chemically sensitized tabular grains are located at the grain edge. This specificity is assumed to be caused by the high dye concentrations present (80–100% monolayer) during the chemical sensitization. In addition, studies of tabular grains have shown that, when sensitized in the presence of dye, the latent image forms at or near the tabular grain edges. An example of this behaviour is shown in Fig. 3.[16] The present authors do not have such data for the emulsions that are the focus of this study, but assume that they would behave similarly.

Although the tabular grains contain adsorbed dye, this has been neglected in the simulations. Volume absorption is used, and any hole trapping provided by the dye is neglected. This seems reasonable for the dyes used in these emulsions.[17] Also, because the run times can be long, particularly for the deeper trap cases, the simulations use an ensemble size of 200 'grains'.

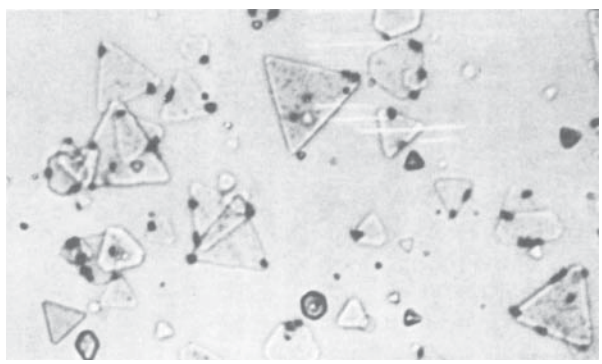

3 Optical micrograph of partially developed tabular grains showing that development is initiated at or near edge of grain; partial development accomplished by developing 1 or 2 min in colour developer (From Hamilton[16])

3 RESULTS AND DISCUSSION

3.1 Unsensitized emulsion

The starting point for the simulations is the correct simulation of the unsensitized emulsion. The B220 emulsion of the companion experimental study[3] is used as a guide. This emulsion has significant internal image. Hence, the model space included an inner core to allow simulation of the internal image. The grain dimensions are 1.2×0.2 μm and the core has dimensions 1.1×0.05 μm, simulating a twin plane separation of 50 nm. The trap depths are 0.05 eV for both surface and twin plane traps. The densities of these traps were adjusted to give the approximate QS and proper onset of LIRF, as compared with the experimental data. The results are shown in Fig. 4.

Both the experimental and simulation results shown in Fig. 4 are for total image — internal plus surface development (see companion paper for details[3]). The simulated QS is about 45 absorbed photons/grain at the high-irradiance end of the reciprocity failure curve, compared with 35–55 absorbed photons per grain estimated for the experimental emulsion at the same exposure time. Both the onset of LIRF and its slope are adequately simulated by the procedure described above. Also, the simulations show an internal image with more speed than the surface image, as seen experimentally for the B220 emulsion.[3]

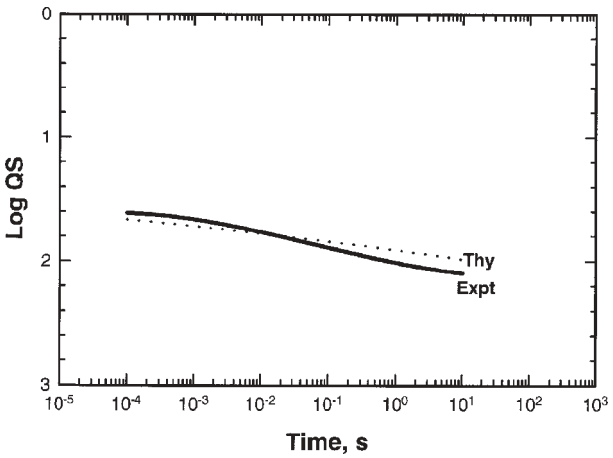

4 Experimental (solid) and simulated (dotted) reciprocity failure curves for unsensitized B220 emulsion; ordinate axis is log QS; experimental curve positioned along this axis to achieve approximate overall match with simulated curve

3.2 Mapping of QS space

Having achieved a good baseline for the unsensitized emulsion, the study then explored how the edge trap depth and trap density, as produced by chemical sensitization, affects the QS of the emulsion. The point of this exercise was to see what maximum efficiencies were possible with given trap depths and densities. These simulations are restricted to 0.1 s exposure, as that seems the most interesting from a practical perspective. Reciprocity failure behaviour of selected trap depth/density combinations will be discussed in a later section.

Figures 5–7 summarize the output of the simulations for grain thicknesses of 200, 100 and 50 nm,

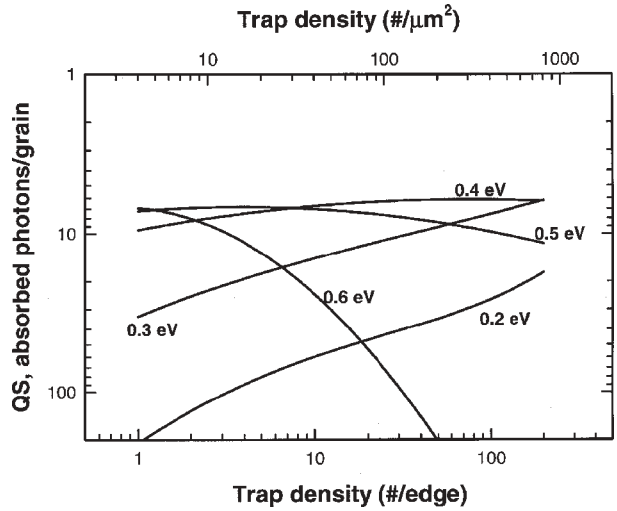

5 QS versus edge trap density for indicated trap depths (0.1 s exposure); grain diameter 1.2 μm; thickness 200 nm

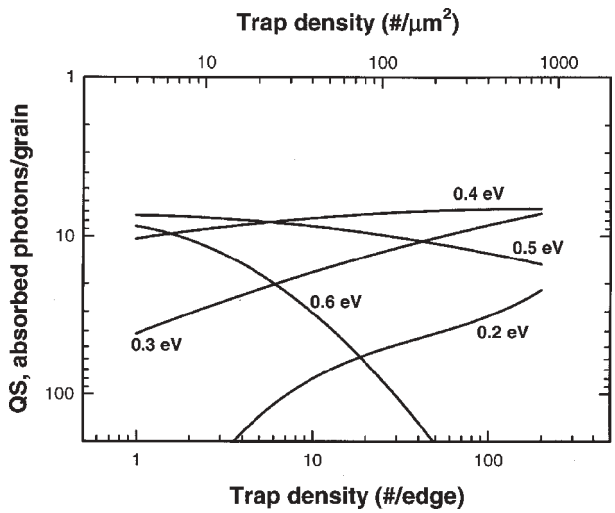

6 Same as Fig. 5 except thickness 100 nm

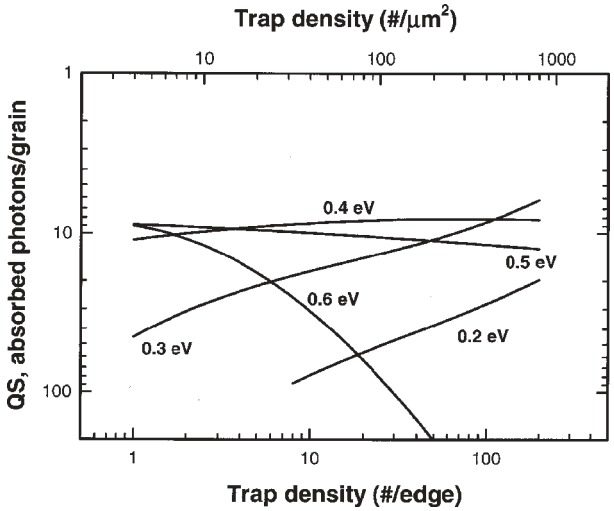

7 Same as Fig. 5 except thickness 50 nm

respectively. In all three cases, the grain diameter is 1.2 μm. The minimum developable size used to determine the QS was three atoms, as this seems to be the size detected in the experimental phase by the developer under normal development conditions.[3] The QS data are plotted versus edge trap density using two units of trap density. In the bottom axis of each figure, the density per edge is used (multiply by four to get the number per grain). In the top axis, a more conventional unit of number per square micrometre is used. The core thickness was lowered to 20 nm in the case of the 50-nm-thick grain to simulate the expected smaller twin plane separation.

Although the unsensitized case is dominated by internal image, this quickly changes with the introduction of deeper edge traps. For 0.3–0.6 eV traps, even a single trap per edge is enough to shift latent-image formation entirely or almost entirely to the edge. For 0.2 eV traps, a trap density of 50 per edge is needed to achieve a similar edge domination.

As expected from earlier work, the QS is very dependent on the trap depth and density.[18] Maximum efficiency is six to eight absorbed photons per grain, and this can be achieved for all three thicknesses with certain trap depth/density combinations. These results serve to emphasize the trap depth/density trade-off in achieving a given QS. For example, for the 200-nm-thick case, a QS of six to eight photons/grain can be achieved with 0.5 or 0.6 eV traps at very low density, or 0.3 or 0.4 eV traps at much higher density. Perhaps even 0.2 eV traps would also reach this value at trap densities higher than those studied. The decrease in efficiency with increasing trap density for the 0.5 eV case, and even more so for the 0.6 eV case, nicely demonstrates the classical oversensitization feature discussed above.

The data given in Figs 5–7 are replotted in Figs 8 and 9 at a constant trap depth, so one can see more clearly the effect of grain thickness on QS. For 0.3 and 0.4 eV trap depths and at constant trap density, the efficiency decreases as the thickness decreases. However, in the 0.4 eV case, the differences are small. For 0.5 and 0.6 eV trap depths, the trends are different. At 0.6 eV, the thinner grains are more efficient. The 0.5 eV case has very little thickness dependence and appears to be a transition case between the 0.3 and 0.4 eV cases and the 0.6 eV case.

Repeating these simulations at high irradiance (10^{-6} s) produced different results for the 0.3 and 0.4 eV trap depth cases. The thickness effect disappeared, indicating that the differences seen at 0.1 s were due to differences in the onset of LIRF. To

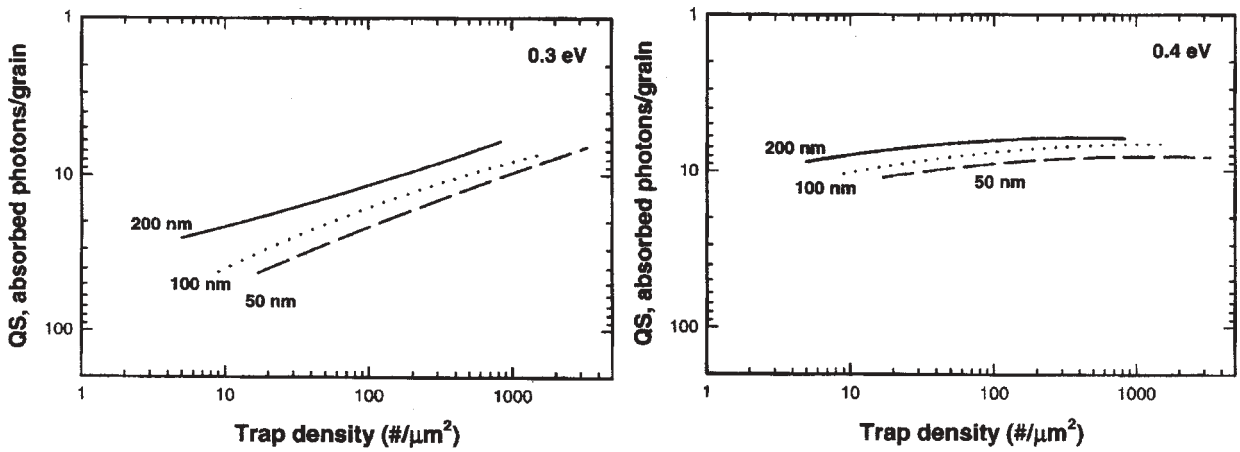

8 QS versus edge trap density for indicated thicknesses at 0.3 and 0.4 eV

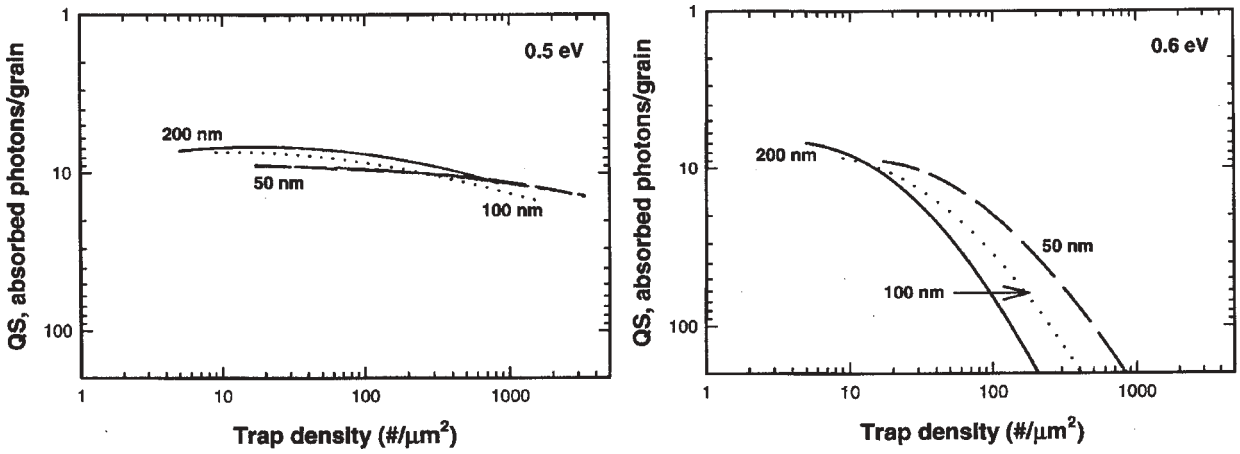

9 Same as Fig. 8 except at 0.5 and 0.6 eV

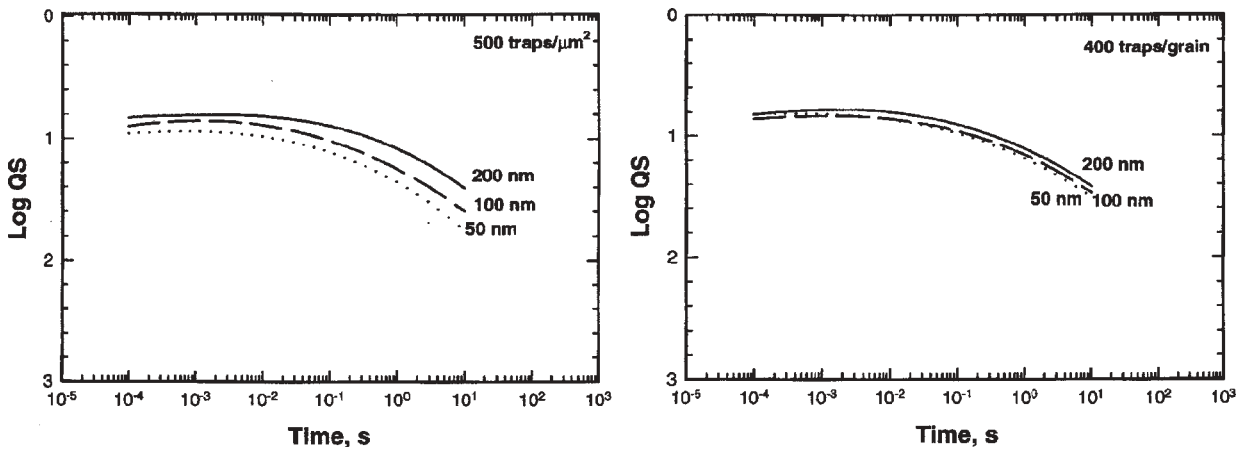

10 Reciprocity failure curves for 200 nm, 100 nm and 50 nm thickness at 0.3 eV trap depth: *left*, constant trap density of 500/μm^2; *right*, constant 400 traps/grain

illustrate this, reciprocity failure curves are presented in Fig. 10 for a 0.3 eV trap depth. The left panel compares the reciprocity failure at a constant trap density of 500/μm^2 and these results indicate an approximate thickness-independent efficiency at high irradiance, but a thickness dependence at low irradiance. The right panel shows the reciprocity failure behaviour for a constant 400 traps/grain. In this case, the thickness dependence virtually disappears, indicating that when the trap density is adjusted to maintain the same number of traps per grain, the efficiency is essentially independent of thickness at all exposure times.

Contrary to the high-irradiance results for the smaller trap depths, the results for 0.5 and 0.6 eV trap depths were the same at 10^{-6} s as for the 0.1 s exposure. At 0.6 eV, the thinner grains continue to be more efficient. This large trap depth leads to oversensitization for all but very low trap densities. In the thinner grains, their smaller volume swings the free/trap hole partitioning toward the trapped side, because holes have a shorter distance to diffuse to the surface where the hole traps are located. This leaves fewer holes for free-hole/trapped-electron recombination which causes oversensitization. As a result, efficiency increases as the thickness decreases.

These simulation results suggest that for trap depths $\leq$0.4 eV, which seem to be the dominant ones observed in the companion experimental study, as the grains are made thinner, the trap depth/density must be changed to maintain constant efficiency. If only the levels of reagents are changed, it is likely that only the number of traps is changed and not the distribution of trap depths.[19–21] In this case, it would be necessary to increase the reagent concentration to maintain a constant number of traps/grain as the thickness decreases. This raises the question as to whether

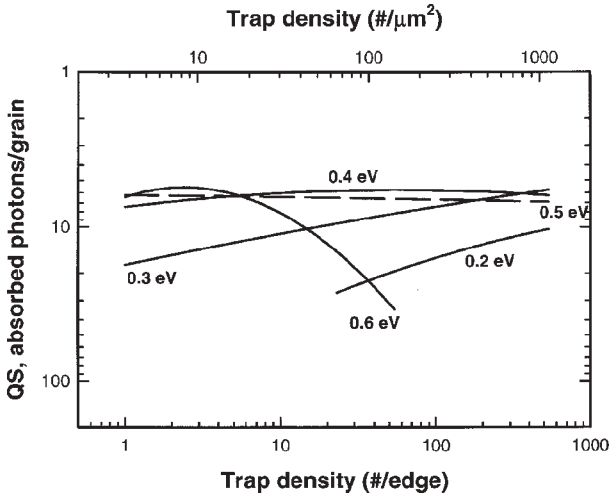

11 QS versus edge trap density for indicated trap depth and for 3.2 μm grain

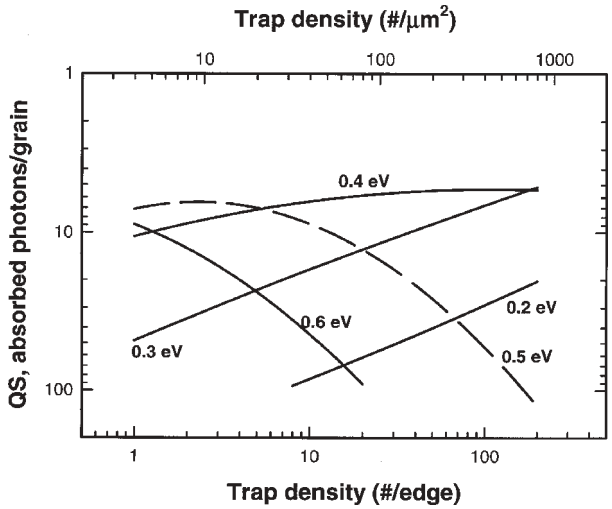

12 QS versus edge trap density for indicated trap depth and for 0.4 μm grain

practically this can be done within the constraints of emulsion stability. Although in practice reagent concentrations are typically increased with decreasing grain size, this is to compensate for the increased surface area/mole as the grain size decreases. The present simulation results suggest that even greater increases in reagent concentration will be needed as tabular grain thickness decreases in order to maintain the same number of traps per edge.

3.3 Diameter effects

Because the tabular grain emulsions are polydisperse, it is of concern how the diameter of the grain affects QS. These simulations were run at 200 nm thickness only and at 0.1 s exposure, as above. The results are shown in Figs 11 and 12 for diameters 3.2 and 0.4 μm, respectively. Although similar maximum efficiencies can be obtained for both sizes, the 3.2 μm grain is generally more efficient than the 0.4 μm grain, being less dependent on the trap density. Figures 13 and 14 give a comparison of QS for all three diameters at a constant trap depth. Figure 13 shows a significant fall-off in efficiency with decreasing diameter for 0.3 eV, but much less so for 0.4 eV trap depth.

These grain diameter effects are inconsistent with what would be expected, based on the experimental data.[22–24] Efficiency of different grain size classes within a polydisperse emulsion is either generally constant for all size classes, or decreases at the larger grain sizes. Likewise, in monodisperse 3D emulsions, the efficiency generally decreases with increasing grain size.[25–29]

These grain diameter effects were studied further by repeating the simulations using a 10^{-6} s exposure. As

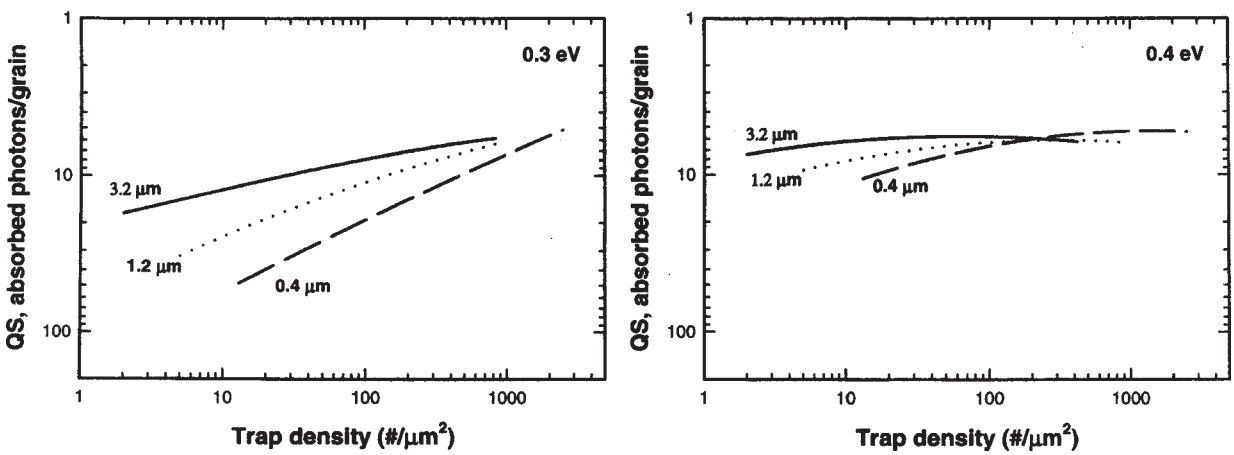

13 QS versus edge trap density for indicated diameters at 0.3 and 0.4 eV

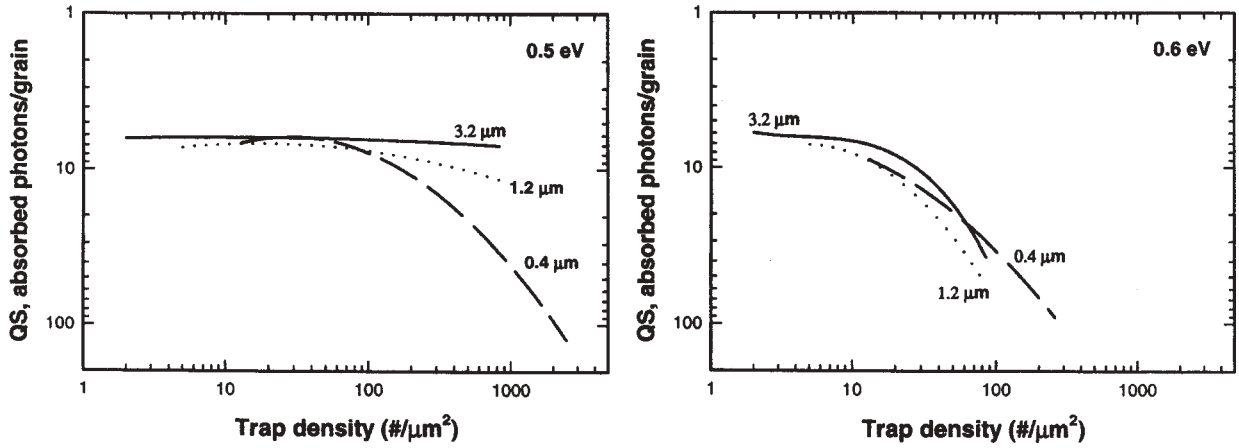

14 Same as Fig. 13 except at 0.5 and 0.6 eV

with the thickness study, at this high-irradiance condition there were no detectable grain diameter effects — all three grain sizes had the same high efficiency of 6 to 8 absorbed photons/grain for all trap density values studied. This result indicates that the effects shown in Figs 13 and 14 are due to reciprocity failure differences among the three diameters studied. Apparently, for a given trap depth and density, the onset of LIRF occurs at shorter exposure times as the grain diameter decreases. Therefore, to maintain constant efficiency over a range of grain diameters, the trap depth or density or some combination of the two must be increased with decreasing diameter. Of course, in a practical experimental situation, this may not be possible when all grain size classes are chemically sensitized in a single emulsion. As a result, the reciprocity failure curve for a polydisperse emulsion is a weighted sum of the reciprocity failure curves of the individual size classes of the emulsion, which may have different onsets for LIRF.

3.4 Reciprocity failure

Reciprocity failure behaviour was simulated for selected parameters using a 1.2×0.1 μm space, and these are shown in Figs 15 and 16 for four different trap depths and a range of trap densities. These data show the expected behaviour from earlier simulations. As the trap depth and/or trap density increases, the reciprocity failure curve is shifted toward longer times so that the time for the LIRF onset increases. In the absence of LIRF, there is only a small difference in efficiency, indicating that much of the QS behaviour seen in Figs 5–9 was induced by changes in reciprocity

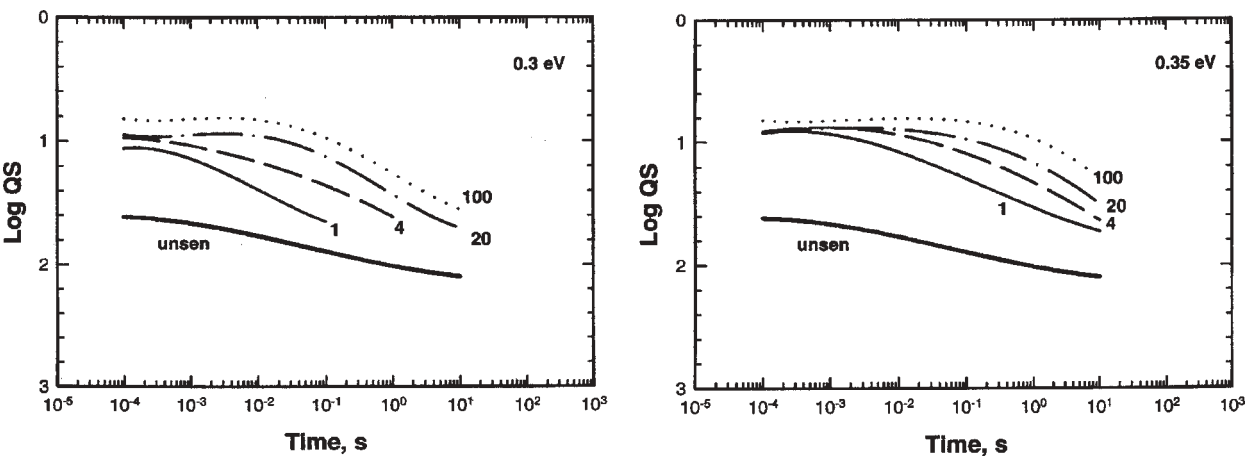

15 Reciprocity failure data for 0.3 and 0.35 eV trap depths; labels on curves give trap density in number/edge; minimum developable size three atoms

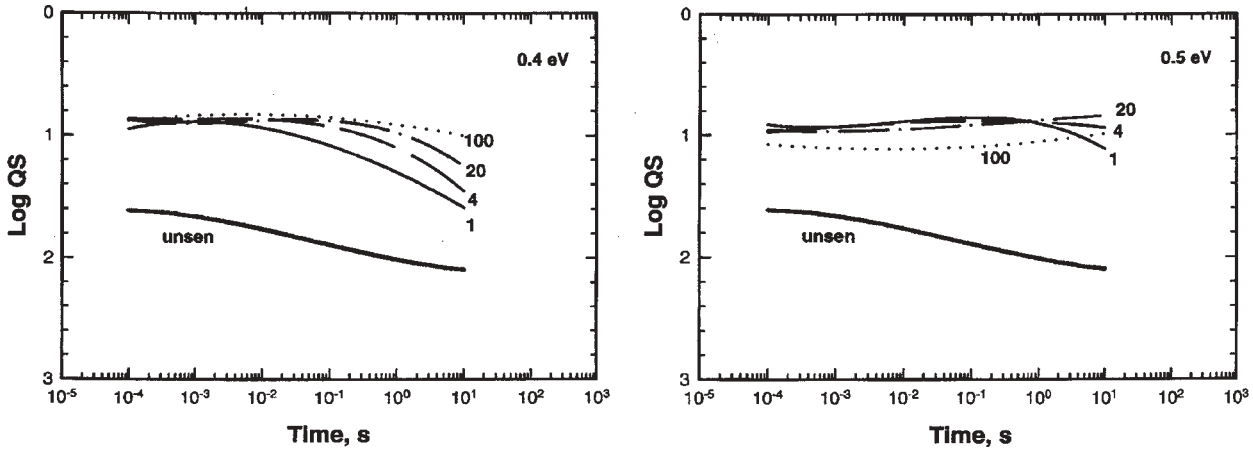

16 Same as Fig. 15 but 0.4 and 0.5 eV trap depths

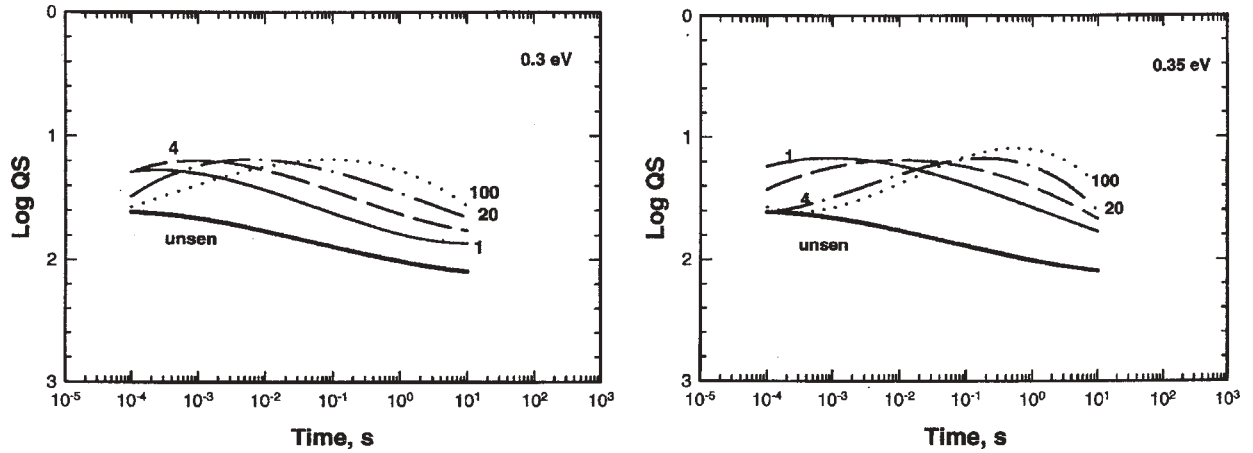

17 Reciprocity failure data for 0.3 and 0.35 eV trap depths; labels on curves give trap density in number/edge; minimum developable size four atoms

failure characteristics, consistent with the effects seen for varying thickness or diameter.

The data in Fig. 17 pertain to a minimum developable size of four atoms. As expected, there is appreciable HIRF for all but the lowest trap density.[18] The curves again shift towards longer time as the trap depth and/or density increases.

3.5 Validation

Armed with these simulation results, one can attempt a comparison with the experimental data. The experimental reciprocity data to be simulated are those for the B220 emulsion. Figure 18 gives a comparison with the simulated data using three trap depth/density combinations that seem to give a good match. Note that the simulated curves for the sensitized emulsions are given without further adjustment of the ordinate

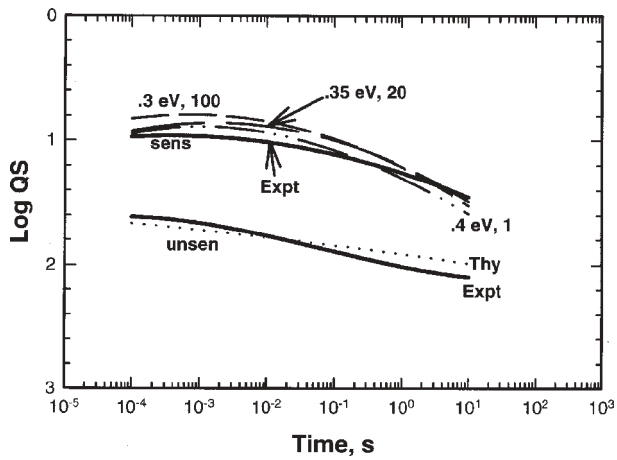

18 Comparison of experimental (B220) and simulated reciprocity failure; experimental curves shifted along speed axis until unsensitized curve approximately matched simulated unsensitized curve; curve labels give trap depth/density (number/edge) combination used in simulation

axis values. Although the simulation data are for 100 nm thickness, at these trap depth/density values there is only a small dependence of QS on thickness.

The comparisons in Fig. 18 show that the experimental trends can reasonably be simulated using the indicated trap depth/density combinations. The main discrepancies are that the simulated efficiency of the sensitized emulsion is a bit too high at the high-irradiance end, and the LIRF slope is a bit too high. Trap depths of 0.5 eV (and by extrapolation 0.6 eV) can be ruled out because they are unable to give a LIRF onset anywhere close to the experimental data, even at the lowest trap density. However, it may be possible that a 0.2 eV trap depth would also work at very high trap densities.

One must be careful in making conclusions from the experimental versus simulation results in Fig. 18, because other parameters can also affect the position of the reciprocity curve with respect to the time axis. One of these is the atom formation time, i.e. the time for an interstitial silver ion to move to the site of the trapped electron. These simulations have used a value of 10^{-5} s, which is close to that expected if there were no space charge layer. This seems reasonable because the experimental emulsions have high stabilizer concentrations which reduce the ionic conductivity to probably near bulk levels.[30]

In the case of the chemically sensitized emulsions, however, one may have to consider the possibility that the sensitizer centre incorporates interstitial silver or gold ions which may be used to form silver or gold atoms.[31–34] Thus, there may be no direct bearing of the ionic conductivity of the emulsion on the atom formation time in this case, and this time may be much shorter than assumed. The reciprocity curve shifts one decade toward longer time for each 10-fold reduction in the atom formation time.[10] Depending on the trap depth/density, the QS at high-irradiance may also be affected. If the atom formation time were shorter, one would need to use lower trap depths and/or densities than those in Fig. 18 to achieve a good fit with experimental data.

Another parameter that affects the lateral position of the reciprocity failure curve is the atom decay time.[10] For each 10-fold increase in decay time, the reciprocity failure curve shifts one decade toward longer time. These simulations use 10^{-4} s as the decay time. It does not seem likely that the atom is less stable than this, but perhaps the atom could be more stable. Again, the high-irradiance QS may also change with increasing decay time. This latter possibility would require a similar adjustment in trap depth/density, as discussed above for a decrease in atom formation time.

In the companion paper describing the experimental phase of this project,[3] an energy-level diagram is constructed using the results of the long wavelength sensitivity measurements on emulsions sensitized in the absence of adsorbed dye. It is argued that the 650 centres and the 750 centres are the important ones for determining the sensitometry, and that the 650 centre was probably the dominant one in terms of concentration. Although the data for emulsions sensitized in the presence of dye were not so easily interpreted, the behaviour for the B220 emulsion used in these simulations was quite similar to that of the undyed emulsions, with a trap depth probably somewhat shallower. Therefore, the mean trap depth for the B220 emulsion sensitized in the presence of dye is probably in the range 0.2–0.4 eV, although no data are available concerning the absolute trap density. It is interesting that the same trap depth range deduced from the experimental data gives reasonable simulation fits to the experimental QS and reciprocity failure data.

4 CONCLUSIONS

Similar to earlier simulations of latent-image formation in three-dimensional grains, high efficiencies for latent-image formation in tabular grains could be achieved with a variety of trap depth/trap density combinations. Simulated QSs for 0.1 s exposure were a function of grain thickness when compared at constant trap density, but were independent of this parameter when compared at constant number of traps/grain. Simulated QSs were also a function of grain diameter at 0.1 s exposure when compared at constant trap density, but not at high irradiance, indicating the exposure time for onset of LIRF decreased with decreasing grain diameter (volume). In this computer simulation study, it was learned that it is possible to fit experimental QS and reciprocity failure data of a tabular-grain AgBr emulsion with a simulation model using trap depths that have been determined experimentally. This provides a qualified validation of the model. Uncertainties remain, because there are processes that affect reciprocity failure whose parameter values are not known accurately, although best guesses have been used.

REFERENCES

1 Kofron, J. T., Booms, R. E., Jones, C. G., Haefner, J. A., Wilgus, H. S. and Evans, F. J. US Patent 4,439,520, 27 March, 1984.
2 Daubendiek, R. L., Black, D. L., Deaton, J. C., Gersey, T. R., Lighthouse, J. G., Olm, M. T., Wen, X. and Wilson, R. D. US Patent 5,503,971, 2 April, 1996.
3 Hailstone, R. K., French, J. and De Keyzer, R. *Imag. Sci. J.*, 2004, **52**, 151.
4 Hailstone, R. K. and De Keyzer, R. *J. Imag. Sci. Technol.*, 2001, **45**, 388.
5 Hailstone, R. K. and De Keyzer, R. *J. Phys. Chem. B*, 2001, **105**, 7533.
6 Berry, C. R. *J. Photogr. Sci.*, 1970, **18**, 169.
7 Ohzeki, K., Urabe, S. and Tani, T. *J. Imag. Sci. Technol.*, 1990, **34**, 136.
8 Zou, C., Sahyun, M. R. V., Mueller, M. E., Levy, B. and Zhang, T. *J. Imag. Sci. Technol.*, 1995, **39**, 106.
9 Hailstone, R. K. *J. Phys. Chem. B*, 1995, **99**, 4414.
10 Hailstone, R. K. *Comput. Phys.*, 1994, **8**, 205.
11 Hamilton, J. F. *Photogr. Sci. Eng.*, 1982, **26**, 263.
12 Hailstone, R. K., Liebert, N. B. and Levy, M. *J. Imag. Sci.*, 1990, **34**, 169.
13 Hamilton J. F. *Photogr. Sci. Eng.*, 1972, **16**, 287.
14 Pouradier, J. In *The Theory of the Photographic Process* (Ed. T. H. James), 1977, 4th edition, p. 74 (Macmillan, New York).
15 Moisar, E. *Photgr. Korr.*, 1970, **106**, 10.
16 Hamilton, J. F. *Adv. Phys.*, 1988, **37**, 359.
17 Zheng, J. P., DiFrancesco, A. G., Hailstone, R. K., Callant, P. and De Keyzer, R. *Imag. Sci. J.*, 2002, **50**, 63.
18 Hailstone, R. K. *J. Imag. Sci. Technol.*, 1995, **39**, 407.
19 Hailstone, R. K., Zhao, T., DiFrancesco, A. G. and Tyne, M. *J. Imag. Sci. Technol.*, 2001, **45**, 76.
20 Hailstone, R. K., French, J. and De Keyzer, R. *Imag. Sci. J.*, 2003, **51**, 21.
21 Hailstone, R. K., French, J. and De Keyzer, R. *Imag. Sci. J.*, 2003, **51**, in press.
22 Farnell, G. C. and Chanter, J. B. *J. Photogr. Sci.*, 1961, **9**, 73.
23 Farnell, G. C. *J. Photogr. Sci.*, 1969, **17**, 116.
24 Broadhead, P. and Farnell, G. C. *J. Photogr. Sci.*, 1982, **30**, 176.
25 Tani, T. *J. Imag. Sci.*, 1985, **29**, 93.
26 Kaneda, T., Oikawa, T., Saeki, N. and Tani, T. In Proc. *IS&T/ SPSTJ Third International East–West Symposium*, Mauui, Hawaii, 1992, paper A-57.
27 House, G. L., Kofron, J. T. and Newmiller, R. J. In the Proc. *SPSE/SPSTJ Second International East–West Symposium*, Kona, Hawaii, 1988, paper B-43.
28 DiFrancesco, A. G., Tyne, M., Pryor, C. and Hailstone, R. K. *J. Imag. Sci. Technol.*, 1996, **40**, 576.
29 Brust, T. B. and House, G. L. *J. Imag. Sci. Technol.*, 1998, **42**, 495.
30 Bi-Xina, P. In Proc. Int. Congr. *Photographic Science*, Cambridge, UK, 1982, p. 171.
31 Tani, T. *J. Imag. Sci. Technol.*, 1995, **39**, 386.
32 Kanzaki, H. and Tadakuma, Y. *J. Phys. Chem. Solids*, 1997, **58**, 221.
33 Van Doorselaer, M. K. and Charlier, E. In Proc. Int. Congr. *Photographic Science*, Antwerp, Belgium, 1998, p. 267.
34 Charlier, E., Van Doorselaer, M. K., Gijbels, R., De Keyzer, R. and Geuens, I. *J. Imag. Sci. Technol.*, 2000, **44**, 235.